GT2010-22482

TOWARDS COOLED TURBINE PRELIMINARY LIFE PREDICTION
via
CONCURRENT AERODYNAMIC, THERMAL & MATERIAL STRESS SIMULATIONS on CONJUGATE MESHES

W N Dawes[1] WP Kellar* & SA Harvey*

CFD Laboratory, Department of
Engineering,
University of Cambridge, Cambridge
CB2 1PZ, UK
&
*Cambridge Flow Solutions Ltd,
Compass House, Vision Park, Cambridge, CB24 9AD, UK

Abstract

An important aspect of the successful design of a cooled turbine blade is trading off performance over a range of disciplines and over a range of conflicting criteria. This in turn implies a need for a speedy & integrated analysis system. The main novelties of the present work are to show: firstly, how the aero, thermal and material stress equations can be conveniently solved on a unified mesh; and secondly, how a very simple but fully integrated process can be constructed for conjugate analysis. As an example of the potential value of this approach, some indicative life predictions for a cooled turbine blade and a shrouded rotor blade will be presented.

Introduction

Cooled HP turbine blade designs must achieve ever higher levels of performance – and must do so in ever shorter time scales. Figure 1 shows an overview sketch of the issues faced: complex physics – aero, thermal and mechanical/material – in complex geometries. With the focus not just on aero-thermal performance but also on weight, life and maintainability, design must be interdisciplinary. The key to a successful design is trading off performance over a whole range of potentially conflicting criteria. Interesting and encouraging work is starting to appear showing the value of these interdisciplinary trades; see for example Dulikravich *et al* [1], Amaral *et al* [2], Verstaete *et al* [3] and Campos-Amezcua *et al* [4]
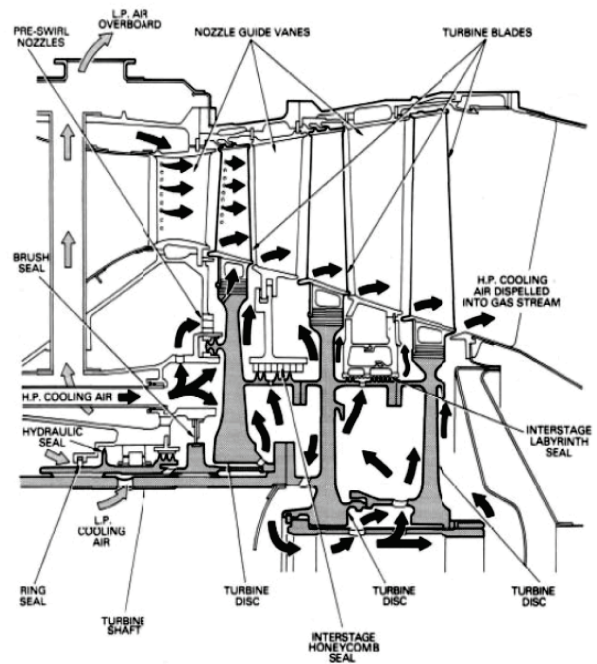

Fig1: Turbine cooling overview

[1] wnd@eng.cam.ac.uk

This interdisciplinary trend in turn implies a need for speedy and integrated analysis tools to permit appropriate trade-off optimization to be performed. Whilst there will always be a role for low order modeling based on correlation (like Kenney *et al* [5] for example), it is becoming important to bring to bear higher order, higher fidelity modeling earlier in the design process – and this has as pacing item the ability to manage and mesh higher fidelity geometry representations.
.
Current high fidelity simulation toolsets, CFD, FEA and so on, have perfectly acceptable performance individually but less so when coupled together in an integrated process. This "process" can be cumbersome, inflexible and dominated by low value-added activities like mesh generation, scripting of the selected analysis packages and data filtering & transfer between different air- and metal-side mesh systems. It would be useful to make all of this interdisciplinary simulation simpler so it can be used earlier in the design cycle and used much more frequently in the design process. This in turn implies a better integrated workflow. Davison *et al* [6] have shown how aero/thermal/mechanical simulation can be performed concurrently on conjugate meshes. In this paper we go a step further to show how the entire simulation process can integrated into one seamless workflow – and how life prediction might be included.

Accordingly, the objectives and main novelties of this paper are to demonstrate that solving the various physical equations for aero, thermal and material stress behavior on a unified mesh leads to a very simple and efficient approach to integrated, conjugate analysis which can easily be implemented on parallel computer systems. This is then extended towards the actual life prediction of the components themselves using standard material properties for creep and fatigue. As an example of the potential value of this approach, the life prediction of a generic cooled turbine blade will be presented followed by a similar study of a generic un-cooled but shrouded turbine blade.

Overview of our integrated simulation system

Algorithmic architecture

The software system, BOXER, represents an attempt to integrate the whole CFD Process "end-to-end" from CAD import through mesh generation, flow solution & post-processing - including the ability to edit the geometry. BOXER has been implemented, at least to prototype standard, end-to-end in parallel—including all data flows between functional units.

The work was motivated by exploration of the possibilities offered by the integration of the solid modeling directly with the mesh generation & with the flow solution—this research combined ideas from solid modeling (see for example Samareh [7,8] & Haimes *et*

al [9]) with virtual sculpting (see for example, Galyean *et al* [10], Perng *et al* [11] and Baeretzen [12]) combined in the context of a simple, cut-Cartesian mesh flow solver (see Bussoletti *et al* [13] or Aftosmis *et al* [14]). A series of publications, Dawes [15, 16, 17], first set out these building blocks and showed their potential as a rapid prototyping design tool and then showed how these building blocks could be efficiently implemented in parallel.

The backbone of BOXER is a very efficient octree data-structure acting *simultaneously* as a search engine, as a spatial occupancy solid model and as an adaptive, unstructured mesh for the flow solver. This provides unlimited geometric flexibility and very robust mesh generation.

The solid model is initialised by the import of a tessellated surface from a variety of potential sources (most CAD engines have an STL export) or by direct interrogation of the CAD solid model kernel itself (Haimes *et al* [9]). The solid model is captured on the adaptive, unstructured Cartesian hexahedral mesh very efficiently by cutting the tesselated boundaries using basic computer graphics constructs developed for interactive 3D gaming. This geometry capture is very fast; for example, a body represented by about 1M surface triangles can be imported into a mesh of around 11M cells (with 6-7 levels of refinement) in approximately 2 minutes on a single, top-end PC. The spatial occupancy solid model is sampled as a distance field and managed as a Level Set; this forms a solid modeling kernel to support the activities of the code.

The BOXER flow solver, based on earlier work on unstructured algorithms [18] is integrated within the software system closely coupled to the solid model and the mesh generation.

Conjugate meshes

A natural result of the meshing methodology (see [15]) is the simultaneous production of conjugate air-side/metal-side meshes connected with a conformal interface as illustrated in Figure 2.
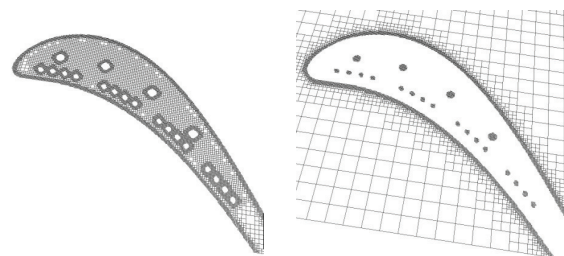

Fig2: Example conformal conjugate meshes; the air-side mesh and the metal-side mesh are produced simultaneously as part of the basic octree mesh generation process [15].

The mesh scale and density is essentially the same both on the air- and the metal-side. This type of mesh is the norm for CFD simulations where many, "low-order elements" are used but is not usual for the metal-side where conventionally a rather coarser mesh of higher order elements is deployed. However, the physical spatial length scales of both air pressure & temperature and material stress variation are by definition the same and it is one of the main contributions of this paper to show that if a high element count, low order discretisation approach is adopted on the metal-side then there is the potentially large benefit of permitting a very simple, easily integrated process.

The next sections will show, in the context of a simple test case, how the air- and metal-side equations are discretised, iteratively solved and integrated

The first case study: mid-span section of an HPT rotor blade

The first case study uses the ACE/RD transonic HPT rotor blade tested in a cascade in the Whittle Laboratory by Haller [19]. Basic parameters are shown in the Table below.

Inlet flow angle	56 deg
Exit flow angle	-65 deg
Exit Mach number	0.90
Reynolds number	2.e+05

Table 1: Basic parameters of the ACE/RD blade

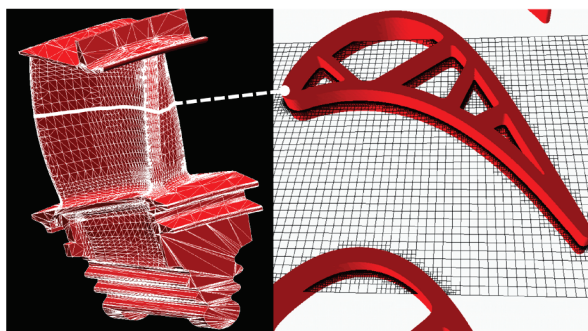This blade is representative of the mid-span of the first stage HP turbine as illustrated in Figure 3.

Fig.3: The mid-span section of an HPT rotor – the ACE/RD blade

The air-side flow solver

Overview

The basic solver is based on earlier work on unstructured meshes (the NEWT code – see Dawes [18]) and can be summarised as:

- second order finite volume
- time marching
- simple mixing length turbulence model
- low-Mach number preconditioning
- agglomeration multi-grid

The basic algorithm was generalised to permit hanging nodes in the h-2h octree mesh transitions to be handled seamlessly. Special boundary conditions were added for the cut cells which are treated via ghost cells combined with local body normals (derived from the distance field) allowing the full shape and curvature of the body to be respected. Classical wall functions (see Launder [20]) are then used to fill these ghost cells.

Application to the test case

The first simulation reported in this paper aims to show the basic air-side performance of this rather simple solver (only about 250 lines of code). As well as comparison with data, simulations were performed using FLUENT on the same mesh as the BOXER solver but exported in body-conformal form – as described in [17]. The basic mesh is shown in Figure 4.
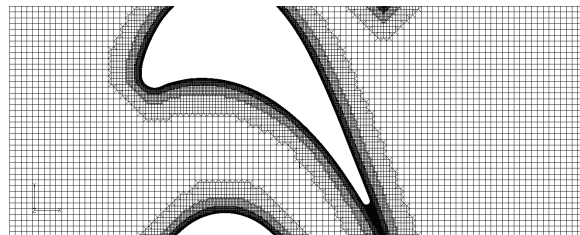

Fig.4: Basic mesh

Figure 5 compares the BOXER simulations with those from FLUENT in terms of Mach number; Figure 6 makes an entropy comparison; and Figure 7 compares predicted and measured blade surface isentropic Mach numbers. The agreement is felt to be satisfactory. Table 2 shows a comparison of loss coefficients – again this was considered encouraging.

Experiment	4.1%
BTOB3d	5.4%
BOXER	6.7%

Table 2: predicted and measured loss coefficients (mass weighted stagnation pressure loss made dimensionless with exit dynamic head)
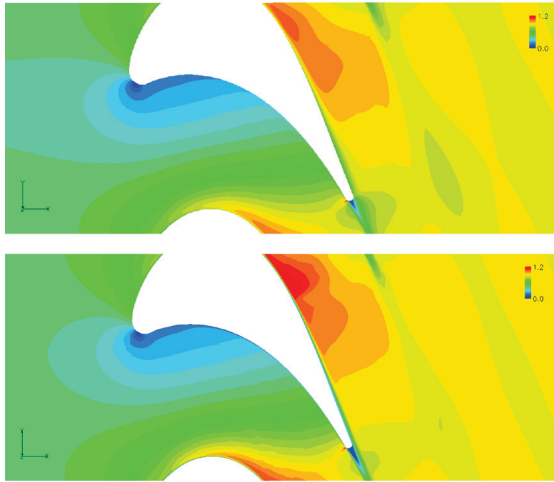
Fig.5: Comparison between BOXER (above) & FLUENT (below): Mach number – range 0 to 1.2

Fig.6: Comparison between BOXER (above) & FLUENT (below) : scaled entropy – range 0.5 to 1.0
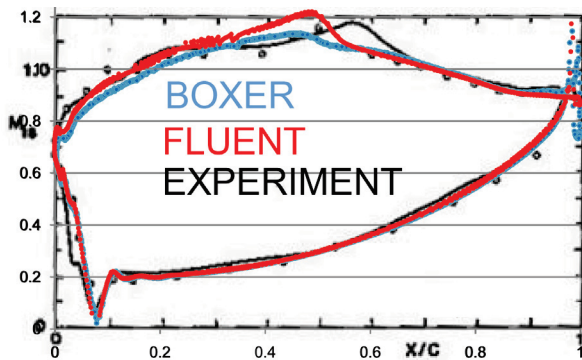

Fig.7: Blade surface isentropic Mach numbers – comparison between data and predictions

The conjugate heat transfer solver

Overview

On the metal side the classic heat transfer conduction equation is:

$$\rho c_p \frac{\partial T}{\partial t} = -\lambda \nabla^2 T$$

This can be readily discretised in finite volume form on the conjugate, cut-Cartesian mesh and solved with simple, explicit time-marching (with the option of agglomeration multi-grid):

$$T^{n+1} = T^n - \Delta t \frac{\lambda}{\rho c_p} \nabla^2 T^n$$

This can be trivially implemented in parallel and uses very little additional computer storage compared to the flow solver.

The key aspects of the conjugate heat transfer solution are the air-metal boundary conditions and the coupling. Figure 8 sketches the approach used. The cut cells are handled via a ghost method with the local wall normal ensuring a body-aligned flow and, in conjunction with the first off-wall flow cell, supporting a classical wall function (see for example Launder [20]) for both the skin friction and wall heat transfer. This use of wall functions is certainly a weakness of the present approach and will be improved in future work. Provision can also be made for Thermal Barrier Coating (TBC) via an additional heat transfer coefficient. Following [21] the temperature fields on the air-side, in the ghost cell and on the metal side are updated simultaneously with the wall heat flux acting as the coupling link. Convergence can be enhanced by having an inner loop for the conjugate cells performing 10-100 iterations for every air-side iteration.
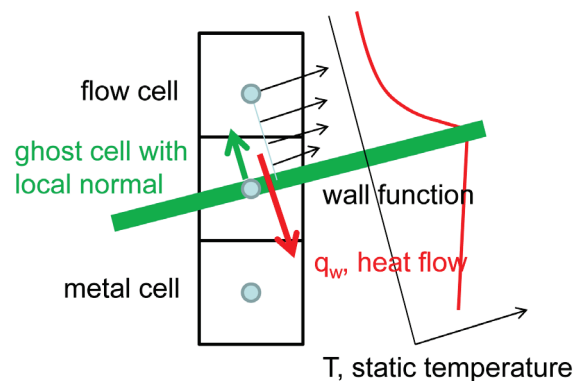

Fig.8: The air-metal boundary conditions for CHT

Heat transfer performance

As a very basic indication of the air-side thermal performance the predicted Nusselt number for the un-cooled blade (as in Figures 4-7) is compared in Figure

4

9 with un-cooled test data from Abhari et al [22]. The agreement is judged adequate – the main problems are at the LE where the wall function fails to predict the local but large spike and the lack of transition modeling. Getting the air-metal HTC right is key to a successful, useful CHT analysis. All CHT methodologies are vulnerable to this and the current work is no exception; this certainly needs to be improved in future work.
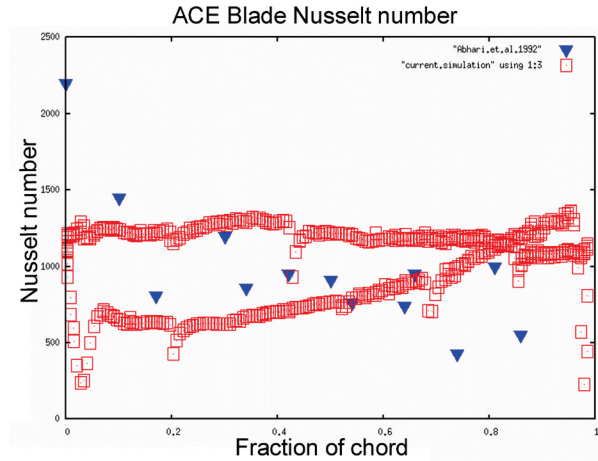

Fig.9: Predicted blade Nusselt number (red) compared with data from Abhari et al [21] (blue)

The conjugate elastic stress solver

Overview

Also on the metal-side, the elastic stress equations are discretised and solved. The classical equations for linear, homogeneous, isotropic elasticity are well known (see for example [23]) and are as follows.

Stress and strain are related by Hooke's law:

$$\boldsymbol{\sigma} = [C]\boldsymbol{\varepsilon}$$

where:

$$[C]^{-1} = \begin{bmatrix} 1/E & -\nu/E & -\nu/E & 0 & 0 & 0 \\ -\nu/E & 1/E & -\nu/E & 0 & 0 & 0 \\ -\nu/E & -\nu/E & 1/E & 0 & 0 & 0 \\ 0 & 0 & 0 & 1/\mu & 0 & 0 \\ 0 & 0 & 0 & 0 & 1/\mu & 0 \\ 0 & 0 & 0 & 0 & 0 & 1/\mu \end{bmatrix}$$

with E Young's modulus and ν Poissons ratio. The strain tensor $\boldsymbol{\varepsilon}$ is defined in terms of the material displacement $\mathbf{u}$ by:

$$\varepsilon_{ij} = \frac{1}{2}\left(\frac{\partial u_i}{\partial x_j} + \frac{\partial u_j}{\partial x_i}\right)$$

and the stress tensor is defined by:

$$\sigma_{ij} = \lambda\varepsilon_{kk}\delta_{ij} + 2\mu\varepsilon_{ij} - 3\alpha\kappa(T - T_{ref})\delta_{ij}$$

where the Lamé constants are:

$$\mu = \frac{E}{2(1+\nu)} \; ; \; \lambda = \frac{E\nu}{(1+\nu)(1-2\nu)}$$

The last term in the stress tensor represents the thermal stresses with T_{ref} a reference temperature, κ the bulk modulus and α the coefficient of thermal expansivity.

A basic force balance in the presence of external force $\mathbf{f}$ leads to the classic elasticity equation to be solved in the presence of appropriate boundary conditions (on a combination of $\mathbf{u}$ and $\boldsymbol{\sigma}$):

$$\rho\frac{\partial^2\boldsymbol{u}}{\partial t^2} + div\,\boldsymbol{\sigma} + \boldsymbol{f} = 0$$

Traditionally this is discretised using a Finite Element methodology with relatively few but high order mesh elements. This is followed by the need to solve a large, sparse matrix problem: [A]$\mathbf{u}$=b. However, this requires a large amount of computer memory – orders of magnitude more than that consumed by a typical flow solver on the same mesh – and can inhibit parallel implementation. This severely restricts the problem size which can be efficiently handled. Whilst there are now sparse matrix solvers implemented in parallel, for example Adams *et al* [24] (which shows structural analysis on meshes with up to 500M DOF on cpu clusters with ~4000 cores in under an hour), it would seem more natural to solve the elasticity equation iteratively (as suggested in [6] for example). Indeed, one of the main novelties of the present work is to show the potential benefits of adopting a very simple solution technique on a mesh unified with the fluid mesh.

Accordingly, in the present work the elasticity equation is discretised in a straightforward finite volume form on a cut-Cartesian mesh and solved using simple time marching (with the option of multi-grid):

$$\boldsymbol{u}^{n+1} = 2\boldsymbol{u}^n - \boldsymbol{u}^{n-1} - \Delta t^2\rho\{div\,\boldsymbol{\sigma} + \boldsymbol{f}\}^n$$

This can be trivially implemented in parallel and uses very little additional computer storage compared to the flow solver. Agglomeration multi-grid can be used to accelerate convergence as well as inner-looping.

The cut cells are handled in a similar way to the air-side using the local body normal to set appropriate ghost cell values; similar approaches for immersed boundary methodologies can be found in the literature, for example Li *et al* [25].

Simple validation: beam stresses

As simple validation of this approach the classical problem of the deflection of a simply supported beam was solved. Figure 10 shows a schematic of the case together with a sketch of the very simple discretisation.

5

For the present second order finite volume approach the number of "degrees of freedom" (DOF) equals the number of cells.
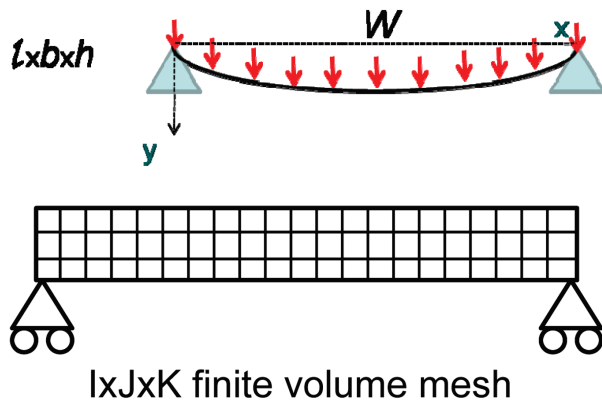

Fig.10: Schematic of the simple beam case: together with the discretisation - DOF, the number of degrees of freedom = IxJxK

The next figure, Figure 11 shows the beam centre-line deflection for three different DOF's made dimensionless with the classical result that the centerline deflection is $(5/384) Wl^3/EI$. As can be seen, as the mesh is refined the analytical result is approached asymptotically.

Figure 12 shows a mesh convergence study: error plotted against log(DOF). Again, it is clear that the error reduces with mesh refinement in the expected way.
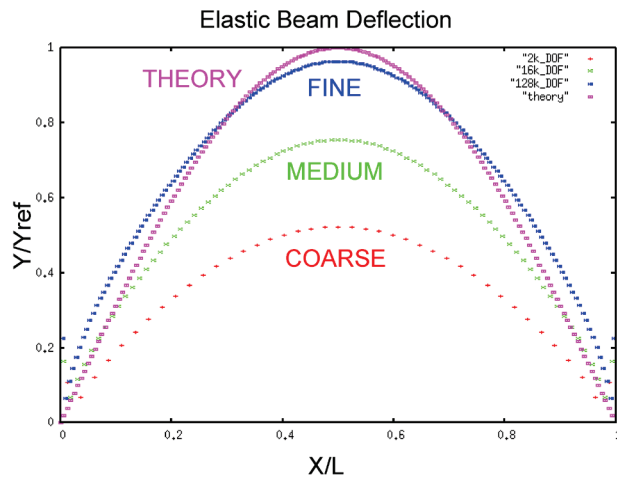

Fig.11: Beam deflection; theoretical result compared to three different mesh sizes: coarse=2k DOF; medium=16k DOF; fine=128k DOF
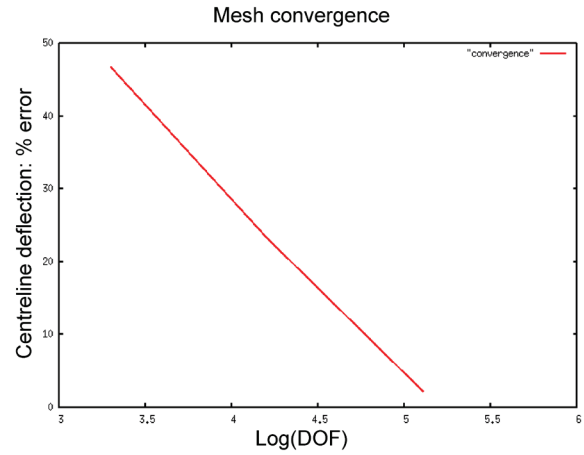

Fig.12: Mesh convergence study; error plotted against log(DOF=degrees of freedom)

Towards life prediction

Overview

Life prediction is a huge and complex subject and needs knowledge not just of the thermal and mechanical status of the blades, disks and shrouds etc. and associated material properties but also operational transients, operating conditions (corrosion etc.) and the cumulative machine history. Understanding and managing life has always been important – often safety critical. However, increasing emphasis on reduced weight (for aero applications) and on better predicting and managing life cycle costs (for "power by the hour" etc.) makes it important to gain understanding of potential life-limiting elements of a design at an early stage.

Accordingly, the objective of this section is very modest: to show how coupled aero-thermal-mechanical analysis might be combined with simple, generic measures of life to give indications of life-limiting issues earlier in the design cycle.

In simple terms there are two life-limiting phenomena *creep*, associated with high temperatures; and *fatigue* associated with frequent load cycling. The description here is taken from a low-order lifing model presented by Oliviero [26].

Creep is associated with high temperatures and the progressive deformation of the material under stress until unacceptable strains have been reached. Creep is governed by an Arrhenius-type law with an activation energy conferring extreme temperature sensitivity. In practical application the industry-standard approach is based on the Larson-Miller parameter:

$$LMP = \frac{T}{1000}(log_{10}t_f + C)$$

where: LMP is the Larson-Miller Parameter; T is the metal temperature; C is a material constant (~20-30); and: t_f is the time to failure in hours. The Larson-Miller Parameter is a function of the background stress level; Figure 13 shows this for Inconel 718.
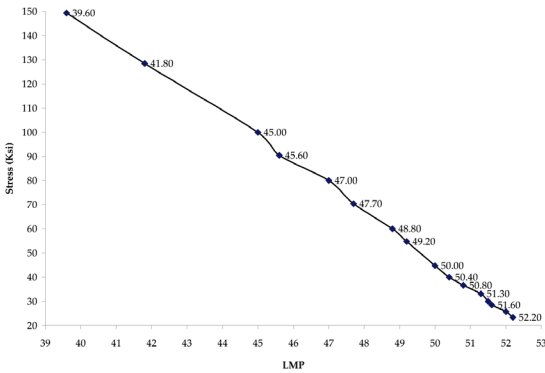

Fig.13: The variation of the Larson-Miller parameter with stress level [26]: the vertical scale is stress level from 20-150ksi; the horizontal scale is for LMP from 39 to 53 .

Fatigue is associated with frequent load cycling which may be mechanical or thermal in origin. The industry-standard approach is the Coffin-Manson method which is correlated by the following "Universal Slope":

$$\frac{\Delta\varepsilon}{2} = \frac{\sigma_f'}{E}(2N_f)^b + \varepsilon_f'(2N_f)^c$$

where: $\Delta\varepsilon/2$ is the cyclic strain range; σ'_f is the fatigue strength coefficient (related to the ultimate tensile strength); ε'_f is the fatigue ductility coefficient; b is the fatigue strength coefficient; c is the fatigue ductility coefficient; and N_f is the number of cycles to failure. The first term represents Low Cycle Fatigue (LCF), the second covers HCF. Values of the various material properties are given in an Appendix for a representative material, Inconel 718. The behaviour of the material is very influenced by statistical effects such as number and distribution of pre-existing cracks and defects. Accordingly, the material constants have a wide variability – and so predictions are really indicative of scaling rather than absolute in nature.

Relative life

Absolute life prediction is a daunting task. The material properties are not known with certainty and the operational history of the turbomachine may not be controllable. Thermal transients are a particular issue as thermal stresses can often dominate mechanical stresses – even those associated with blade rotation (see [4] for example) – if the geometry is constrained in some way and not free to deform. To account for this properly really needs a thermal-mechanical analysis of the whole engine – or at least the local disc-blade-shroud-casing sub-system.

Hence the approach adopted here is to define a *relative life* – the ratio between the life predicted at a given location and the minimum life anywhere in that geometry. The intention is that this will give the designer a clear and three-dimensional indication of where the life is limited – and why – in the hope that the design can be changed.

Application to the first test case: an internally cooled HPT rotor blade

Accordingly, this section presents a demonstration of how *relative life* can be predicted in a simple test case: the mid-span section of an internally cooled HPT rotor blade. A 3D but small spanwise section was modeled and spanwise periodic boundary conditions were used for the flow, thermal and stress fields. A TBC was simulated on the blade surfaces.

The primary path boundary conditions and cooling temperature were set to be representative of cruise. In practice other operating conditions like take-off might also be important in assessing overall life. The effect of several loading schedules could be combined using, for example, Miner's rule [26].

The generic internal cooling system was modeled as follows. Inside the cooling passages a correlated, typical, heat transfer coefficient was applied and the air maintained at a fixed cooling temperature (effectively by removing all heat arriving from the air-side). No passage to passage temperature pick up was specified.

Although the blade was simulated in a cascade this is representative of the real rotating environment where constant rothalpy at constant radius implies constant rotor-relative stagnation temperature.

The reference temperature for the thermal stresses was taken as the mean of the free stream stagnation temperature and the cooling temperature and the thermal stresses dominate the mechanical ones.

Inconel 718 was selected as a representative blade material and the Appendix show the values used for all the material constants.

The results are shown in Figures 14-17. Figure 14 shows the metal-side temperature distribution predicted by the Conjugate Heat Transfer simulation and plotted as $(T-T_{cool})/(TO1-T_{cool})$ with range 0.16 (blue) to 0.83 (red). The distribution of *relative* creep life over the blade section is shown in Figure 15 with range $1=10^0$ at the life-limiting locations (blue) to 10^{23} (red). The creep life is clearly limited by excessive metal temperature in the TE region of the blade.

7

What is notable is the huge spatial variability of life and the huge range – an HPT blade at cruise is hugely sensitive to temperature and very vulnerable to unexpected spatial temperature variations. The obvious implication is that one-dimensional life prediction methods may be very difficult to apply and interpret and hence lead to unnecessarily conservative design.

Also of interest, given the very large spatial variability of temperature (and stress as will be seen) is whether the material properties themselves are valid as things like creep life and so on are usually measured under controlled conditions of uniform temperature and background stress.

Figure 16 shows the corresponding distribution of the dimensionless von Mises stress, plotted as σ/σ_{max}, and with range 0.1 (blue) to 1.0 (red). In this simulation the stress field is dominated by thermal stresses. Figure 17 shows the associated distribution of *relative* fatigue life over the blade section plotted with range $1=10^0$ at life-limiting locations (blue) to $10^{13.7}$ (red). The fatigue life is clearly limited by (thermal) stresses in the internal cooling passage wall and their intersection with the hot blade perimeter.
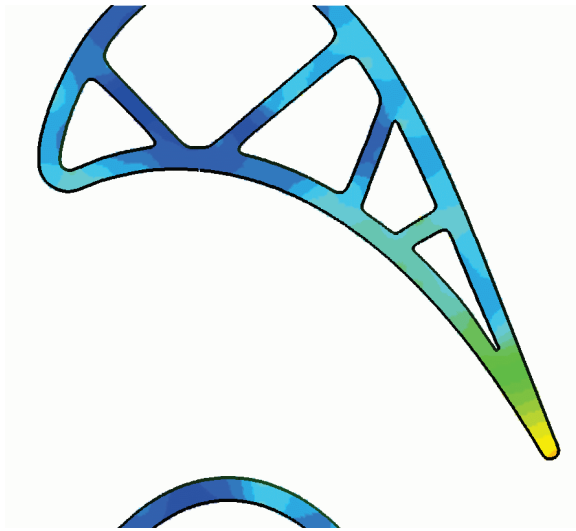

Fig.14: Representative metal-side temperature distribution $(T-T_{cool})/(TO1-T_{cool})$: range 0.16 (blue) to 0.83 (red)
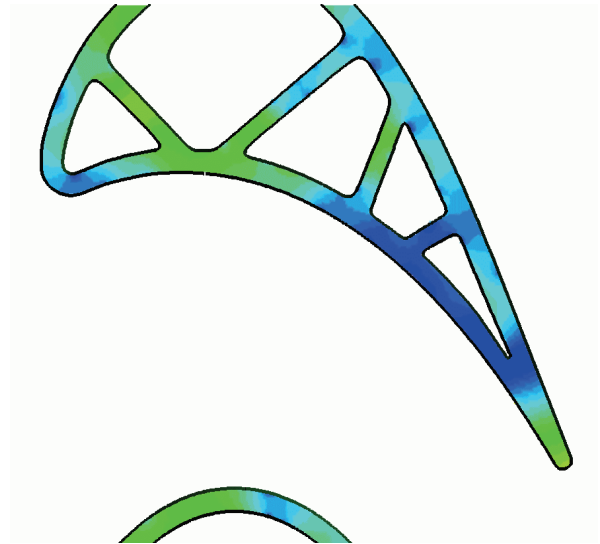

Fig.16: Corresponding distribution of dimensionless von Mises stress σ/σ_{max}: range 0.1 (blue) to 1.0 (red)
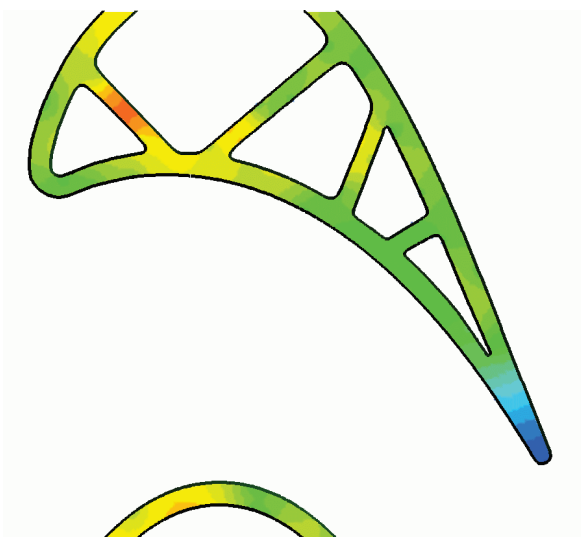

Fig.15: Distribution of relative creep life over the blade section; range $1=10^0$ (blue) to 10^{23} (red)
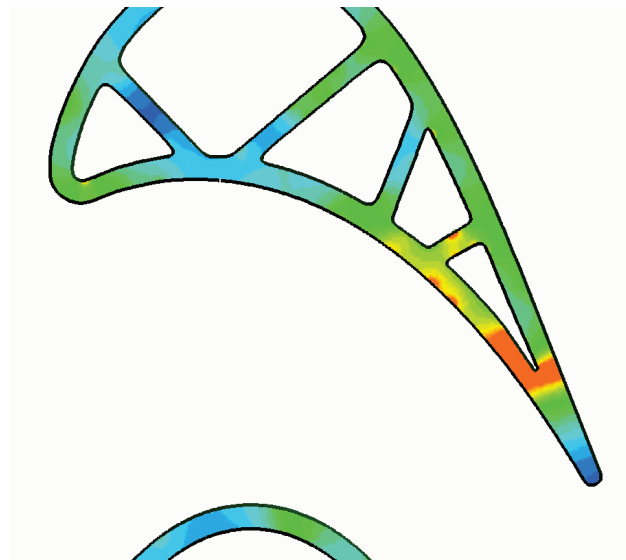

Fig.17: Distribution of relative fatigue life over the blade section; range $1=10^0$ (blue) to $10^{13.7}$ (red)

Again, what is notable is the huge spatial variability of life and the huge range with the life limited at a few critical spatial locations. Again, one-dimensional life prediction methods may be very misleading and overly conservative.

A second case study: a shrouded rotor blade

The second blade selected for this study is not strictly speaking "cooled" but is included to show some rather more three-dimensional aspects of lifing. The blade is a generic, shrouded rotor blade with basic parameters shown in the Table below.

Inlet flow angle	0deg
Exit flow angle	-59 deg
Exit Mach number	0.85
Reynolds number	5.e+05
Inlet stagnation TO	950K

Table 3: Basic parameters of the shrouded rotor blade

Figure 18 shows a view of the CAD model from which the mesh was generated directly. The outboard half of the rotor was simulated and with a modest mesh sized at ~0.5M cells to allow a basic laptop computer to be used. Boundary conditions at the mid-span cut plane were zero heat transfer, zero material strain and a stress field consistent with the rotating mass of the blade and shroud.
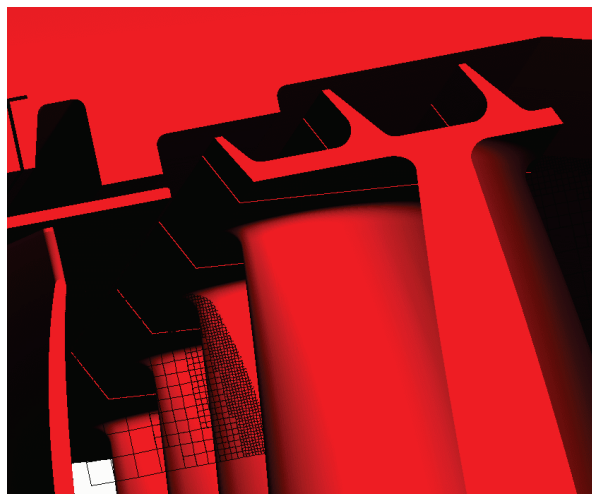

Fig.18 Overview of the CAD model for the generic, shrouded rotor blade

A very brief overview of the aero predictions is given in Figure 19. The blade-blade static pressure field shows a conventional high reaction design. The velocity vectors and Mach numbers for a constant theta cut passing through the blade LE show the expected

over-shroud leakage flow – effectively choked over the shroud fences – and with recirculation in each of the shroud cavities. (The background field colour for the vector plot is static pressure showing how the blade pressure drop is shared across the shroud loss generation sites.) Some castellation is visible on the blade and shroud surfaces – this is a current limitation of our post-processing which does not properly recognize cut cells. However, the solver does use the ghost cell/wall normal approach described earlier to resolve the true body shape.
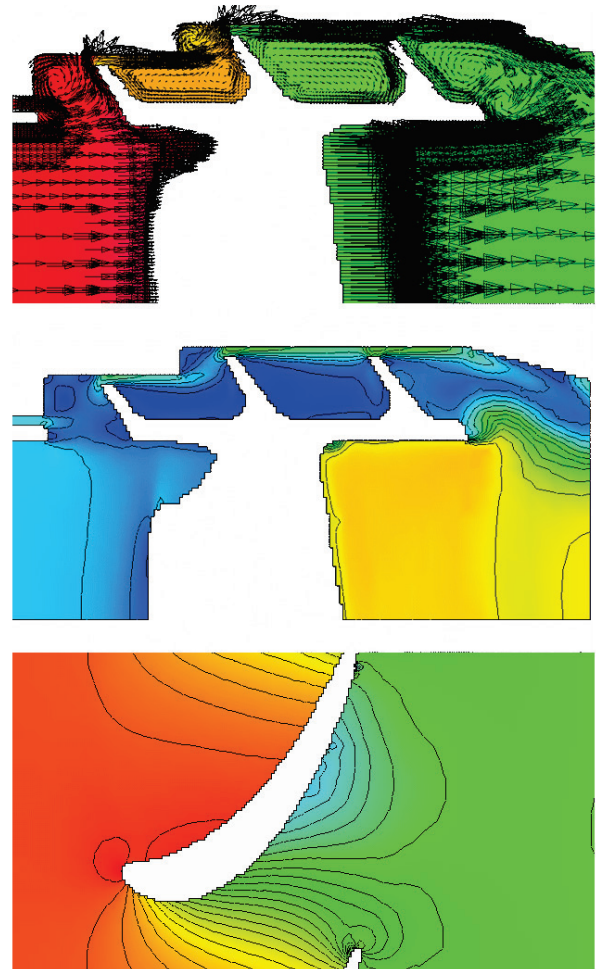

Fig.19: Overview of the aero simulation: (top) velocity vectors for a constant theta cut passing through the blade LE; (middle) Mach numbers in the same cut plane; (bottom) mid-span static pressure field.

The final results relate to the conjugate heat transfer simulation and here we just focus on creep life.

Figure 20 shows, in a cut-plane at constant theta passing through the blade LE, the predicted conjugate temperature distribution (top) with range 883K to 950K and associated relative creep life (bottom) with range

1=10^0 to $10^{4.3}$. Figure 21 shows the same pair of predictions in a mid-span blade-blade cut.

Fig.20: Predicted conjugate temperature distribution (top) with range 883K (blue) to 950K (red) and associated relative creep life (bottom) with range 1=10^0 (blue) to $10^{4.3}$ (red)
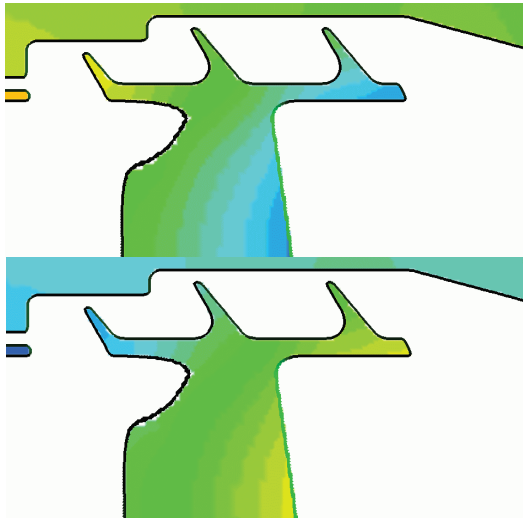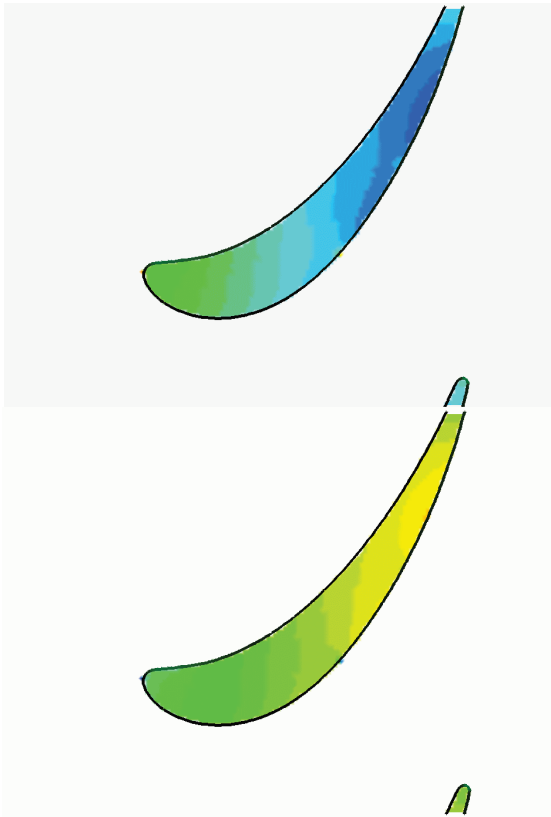

Fig.21: Predicted conjugate temperature distribution (top) with range 883K (blue) to 950K (red) and associated relative creep life (bottom) with range 1=10^0 (blue) to $10^{4.3}$ (red)

As in the previous example it is interesting to observe the large spatial variability of creep life. In this case the life is limited by the leading shroud fence. In practice this might need cooling, perhaps supplied from the stator casing rather than via rotor internals.

Concluding Remarks

This paper has described recent extensions to the BOXER software system to include the integration of aero and conjugate thermal & material stress simulations together on a single, unifying mesh.

Even though some of the physical models we have deployed are clearly place-holders, we believe we have demonstrated the potential benefits of our approach: simplicity; speed; low computer memory consumption; easily parallelizable.

The most serious shortcoming is the prediction of the heat transfer coefficient from the air- to the metal-side and this we will focus on next. Although the high element count on the metal-side might seem to be a disadvantage, in fact in practice this appears not to be the case as the discrete equations are so simple and can be solved so rapidly with little memory overhead.

The two case studies were very simple and would need to be extended at least to the level of a full blade/disk/shroud/casing assembly with the local secondary air system to make a practical contribution to improving life. Nevertheless, the case studies showed that it will be feasible to move beyond basic 1D correlations at an early design stage – concurrent with performing basic blade design - to get some insight into the evidently highly three-dimensional life-limiting phenomena.

In the future this application also in helping manage maintenance & service contracts on engines in the field – possibility combined with on-site condition monitoring - to build a more financially optimum business model for large gas turbines and similar equipment.

Acknowledgements

Appendix: blade material properties

The following properties were used in the simulation:

Density, ρ	8.22 kg/m^3
Thermal conductivity	80.4 W/mK
Young's modulus, E	208 GPa
Poisson's ratio, ν	0.29
Bulk modulus, κ	208 GPa
Thermal expansivity, α	13.5e-06 /K
σ'_f	1.74 GPa
ε'_f	0.35
b	-0.08
c	-0.59
TBC, thickness	0.8 W/mK
& thermal conductivity	0.3mm

Table 4: Material properties for Inconel 718 [26] and a TBC: ZrO2-Y2O3 TBC [27]

References

[1] Dulikravich GS, Denis BH, Martin TJ & Egorov IN "Multi-disciplinary analysis and design optimisation" Invited Lecture, Brazilian Congress on Applied and Computational Mathematics, Bel Horizonte, 2001

[2] Amaral S, Verstaete T, van dem Braembussche R Arts T "Design and optimization of the internal cooling channels of a HP turbine blade – Part I, Methodology" ASME GT2008-51077, Berlin 2008

[3] Verstaete T, Amaral S, van dem Braembussche R Arts T "Design and optimization of the internal cooling channels of a HP turbine blade – Part II, Optimisation" ASME GT2008-51080, Berlin 2008

[4] Campos-Amezcua A, Mazur Z & Gallegos-Munoz A "Thermo-mechanical and transient analysis and conceptual optimization of a first stage bucket" ASME Paper GT2008-51217, Berlin, 2008

[5] Kenny SC, Gaulthier JED & Huang X "Multidisciplinary design tool for axial flow turbines" ASME Paper GT2006-90192, Barcelona, 2006

[6] Davison JB, Ferguson SE, Mendonca FG & Peck AF "Towards an automated simulation process in combined thermal, flow and stress in turbine blade cooling analyses" ASME Paper GT2008-51287, Berlin, 2008

[7] Samareh, JA "Status & Future of Geometry Modelling and Grid Generation of Design and Optimisation" J. of Aircraft, Vol 36, no1, Feb 1999

[8] Samareh JA "Survey of shape parameterisation techniques for high-fidelity multi-disciplinary shape optimisation" AIAA Journal Vol.39, No.5, 2001

[9] Haimes R & Follen GL "Computational Analysis Programming Interface" Proc. 6th Int. Conf. On Numerical Grid Generation in Computational Field Simulations, Eds. Cross, Eiseman, Hauser, Soni & Thompson, July 1998.

[10] Galyean TA & Hughes JF "Sculpting: an interactive volumetric modelling technique" ACM Trans., Computer Graphics, vol.25, no.4, pp 267-274, 1991

[11] Perng K-L, Wang W-T, Flanagan M & Ouhyoung M "A real-time 3D virtual sculpting tool based on modified marching cubes", SIGGRAPH, 2001

[12] Baerentzen A "Volume sculpting: intuitive, interactive 3D shape modelling" IMM, May 2001

[13] Bussoletti JE, Johnson FT, Bieterman MB, Hilmes CL, Melvin RG, Young DP & Drela M "TRANAIR: solution-adaptive CFD modelling for complex 3D configurations" AIAA Paper 1995-0451, 1985

[14] Aftosmis MJ, Berger MJ & Melton JE, "Robust and efficient Cartesian mesh generation for component-based geometry" AIAA J., 36, 6, 952-, 1999

[15] Dawes WN "Building Blocks Towards VR-Based Flow Sculpting" 43rd AIAA Aerospace Sciences Meeting & Exhibit, 10-13 January 2005, Reno, NV, AIAA-2005-1156

[16] Dawes WN "Towards a fully integrated parallel geometry kernel, mesh generator, flow solver & post-processor", 44th AIAA Aerospace Sciences Meeting & Exhibit, 9-12 January 2006, Reno, NV, AIAA-2006-45023

[17] Dawes WN, Harvey SA, Fellows S, Favaretto CF & Vellivelli A "Viscous Layer Meshes from Level Sets on Cartesian Meshes", 45th AIAA Aerospace Sciences Meeting & Exhibit, 8-11 January 2007, Reno, NV, AIAA-2007-0555

[18] Dawes WN "Simulating unsteady turbomachinery flows on unstructured meshes which adapt both in time and space", ASME Paper 93-GT-104, 1993.

[19] Haller BJ "Transonic turbine cascade" PhD Thesis, Cambridge University, 1979

[20] Launder B "Wall-function strategies for use in turbulent flow CFD" Computer Modelling/Simulations for Industrial and Environmental Flows, Workshop, Macerata, Italy, October 2007

[21] Divo E, Steinthorssen E, Rodriguez F, Kassab AJ & Kapat JS "Glenn HT/BEM conjugate heat transfer solver for large scale turbomachinery models" NASA/CR-2003-212195

[22] Abhari RS, Guenette GR, Epstein AH & Giles MB "Comparison of time-resolved turbine rotor blade heat transfer measurements and numerical calculations" Transactions of the ASME, vol.114, pp.818-, Oct.1992

[23] Legace PA "Unit 4: equations of elasticity", MIT 16-20, Fall 2002

[24] Adams MF, Bayraktar HH, Keaveny TM & Papadopoulos P "Ultrascalable implicit finite element analysis in solid mechanics with over half a billion degrees of freedom" Super Computing SC'04, Pitssburgh, PA, 2004

[25] Li Z & Yang X "An immersed FEM for elasticity equations with interfaces" North Carolina State University, Centre for Research in Scientific Computation, Report, August 2004

[26] Oliviero VS "A flexible lifing model for gas turbines: creep and low cycle fatigue approach" MSc Thesis, Cranfield University, 2006

[27] McDonald G & Hendricks RC "Effect of thermal cycling on ZrO2-Y2O3 thermal barrier coatings" NASA TM81480, 1980

-oOo-